J. Fluid Mech. (2023), *vol*. 976, A24, doi:10.1017/jfm.2023.844

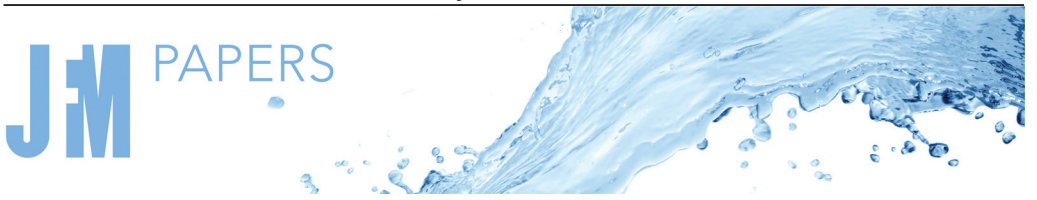

An analytical model of momentum availability for predicting large wind farm power

Andrew Kirby[1],†, **Thomas D. Dunstan**[2] **and Takafumi Nishino**[1]

[1]Department of Engineering Science, University of Oxford, Parks Road, Oxford OX1 3PJ, UK

[2]Met Office, FitzRoy Road, Exeter EX1 3PB, UK

(Received 13 June 2023; revised 22 August 2023; accepted 2 October 2023)

Turbine–wake and farm–atmosphere interactions influence wind farm power production. For large offshore farms, the farm–atmosphere interaction is usually the more significant effect. This study proposes an analytical model of the 'momentum availability factor' to predict the impact of farm–atmosphere interactions. It models the effects of net advection, pressure gradient forcing and turbulent entrainment, using steady quasi-one-dimensional flow assumptions. Turbulent entrainment is modelled by assuming self-similar vertical shear stress profiles. We used the model with the 'two-scale momentum theory' to predict the power of large finite-sized farms. The model compared well with existing results of large-eddy simulations of finite wind farms in conventionally neutral boundary layers. The model captured most of the effects of atmospheric boundary layer (ABL) height on farm performance by considering the undisturbed vertical shear stress profile of the ABL as an input. In particular, the model predicted the power of staggered wind farms with a typical error of 5 % or less. The developed model provides a novel way of predicting instantly the power of large wind farms, including the farm blockage effects. A further simplification of the model to predict analytically the 'wind extractability factor' is also presented. This study provides a novel framework for modelling farm–atmosphere interactions. Future studies can use the framework to better model large wind farms.

Key words: atmospheric flows, general fluid mechanics

1. Introduction

Wind energy is a key technology for the renewable energy transition. To meet future energy demands, wind energy capacity will need to increase rapidly, and individual farms

† Email address for correspondence: andrew.kirby@trinity.ox.ac.uk

will likely become larger (Veers *et al.* 2022). A key aspect for designing wind farms is predicting their power output. However, it is difficult to model the aerodynamics of large wind farms because of the multi-scale nature of flows involved (Porté-Agel, Bastankhah & Shamsoddin 2020).

Traditionally, there are two main approaches to predicting wind farm performance at a low computational cost. For the first approach, semi-analytical 'wake' models predict the velocity deficit in the wake behind a turbine (e.g. Jensen 1983; Bastankhah & Porté-Agel 2014). To model an entire wind farm, individual wakes are superposed using different techniques (e.g. Katic, Hojstrup & Jensen 1986; Zong & Porté-Agel 2020). Wake models are used commonly to optimise the layout of turbines in a farm. However, they do not consider the atmospheric response to wind farms, thus they perform poorly for extended wind farms (e.g. Stevens, Gayme & Meneveau 2016). The second approach uses 'top-down' models (e.g. Frandsen 1992; Frandsen *et al.* 2006; Calaf, Meneveau & Meyers 2010). Top-down models consider the response of an idealised atmospheric boundary layer (ABL) to an infinitely large wind farm. They cannot, however, predict the impact of turbine layout (placement of turbines within a farm) on farm performance. Recent studies have coupled the wake and top-down models together (e.g. Stevens *et al.* 2016; Starke *et al.* 2021). This approach, however, still has the limitations of the constituent models, e.g. idealised ABL profiles and wake superposition methods.

More recently, models have been developed to predict the interaction between wind farms and the atmosphere. Meneveau (2012) extended top-down models to finite wind farms by considering the development of an internal boundary layer. Luzzatto-Fegiz & Caulfield (2018) modelled the impact of entrainment on farm performance by using a three-layer model. This model was extended to finite wind farms by Bempedelis, Laizet & Deskos (2023). Smith (2010) predicted the impact of gravity waves on wind farm performance by solving a two-layer model using fast Fourier transforms. This approach was later extended to a three-layer model (Allaerts & Meyers 2018, 2019). The model was extended further to include the impact of vertically varying free atmospheres (Devesse *et al.* 2022). All of these approaches require solving differential equations numerically to predict wind farm performance.

Nishino & Dunstan (2020) developed the 'two-scale momentum theory' to better understand the power generation mechanism of large wind farms. This splits the multi-scale problem of wind farm aerodynamics into 'internal' turbine/array-scale and 'external' farm/atmospheric-scale sub-problems. The sub-problems are coupled together using the conservation of momentum. As farms become larger, one of the grand challenges facing the wind energy community is to understand the impact of farm–atmosphere interaction (Veers *et al.* 2019). Kirby, Nishino & Dunstan (2022) confirmed this by performing large-eddy simulations (LES) of 50 different periodic turbine layouts. They introduced the concepts of 'turbine-scale losses' due to turbine–wake interactions, and 'farm-scale losses' caused by the atmospheric response to the whole farm. For large offshore farms, the farm-scale losses were found to be typically more than twice as large as the turbine-scale losses. This highlights the importance of modelling farm-scale flows to predict the performance of future large farms.

Unlike most large wind farm models, the two-scale momentum theory does not assume any specific profiles of the ABL (such as a logarithmic law), allowing for the external sub-problem to be modelled in various manners. For the external modelling, it is crucial to predict accurately how the momentum available to the farm site increases due to the presence of the turbines, i.e. the momentum availability. Recent studies by Patel, Dunstan & Nishino (2021) and Legris *et al.* (2023) used 'twin' numerical

weather prediction (NWP) simulations to calculate the momentum availability and thus predict how farm-scale losses (including the so-called farm blockage losses) change with atmospheric conditions. However, this approach would be too computationally expensive for wind farm optimisation unless a sufficiently long set of twin NWP simulations (such as those reported by van Stratum *et al.* 2022) has already been conducted for candidate wind farm sites.

In the present study, we propose a simple analytical model to predict the momentum availability for large wind farms. This model, together with the two-scale momentum theory, allows us to predict the power of a large wind farm analytically. The model is derived using quasi-one-dimensional (quasi-1-D) control volume analysis and assuming self-similar vertical shear stress profiles. In § 2, we summarise the two-scale momentum theory and the key wind farm parameters. Section 3 presents the derivation of the new momentum availability factor model. In § 4, we compare the predictions of farm power with existing finite wind farm LES. The model is discussed further in § 5, and concluding remarks are given in § 6.

2. Two-scale momentum theory

By considering the conservation of momentum for a control volume with and without a wind farm present, Nishino & Dunstan (2020) derived the non-dimensional farm momentum equation

$$C_T^* \frac{\lambda}{C_{f0}} \beta^2 + \beta^\gamma = M. \tag{2.1}$$

Here, β is the farm wind-speed reduction factor, defined as $\beta \equiv U_F/U_{F0}$ (with U_F defined as the average wind speed in the nominal farm layer of height H_F, and U_{F0} the farm-layer-averaged speed without the presence of the turbines); C_T^* is the (farm-averaged) 'internal' turbine thrust coefficient, defined as $C_T^* \equiv \sum_{i=1}^{n} T_i/\frac{1}{2}\rho U_F^2 nA$ (where T_i is the thrust of turbine i, A is the rotor swept area, and n is the number of turbines in the farm); λ is the array density, defined as $\lambda \equiv nA/S_F$ (where S_F is the wind farm area); C_{f0} is the natural friction coefficient of the surface, defined as $C_{f0} \equiv \tau_{w0}/\frac{1}{2}\rho U_{F0}^2$ (where τ_{w0} is the undisturbed bottom shear stress); and γ is the bottom friction exponent, defined as $\gamma \equiv \log_\beta(\tau_w/\tau_{w0})$ (assumed to be 2 in this study). Also, M is the momentum availability factor, given by

$$M = \frac{X - C - \left[\dfrac{\partial p}{\partial x_F}\right] - \dfrac{\partial[\rho U]}{\partial t}}{X_0 - C_0 - \left[\dfrac{\partial p_0}{\partial x_{F0}}\right] - \dfrac{\partial[\rho U_0]}{\partial t}}, \tag{2.2}$$

where U is the velocity in the hub-height wind direction (i.e. streamwise direction) x_F, X represents the net streamwise momentum injection through the top and side boundaries of the control volume (due to advection and Reynolds stress), C is the streamwise component of the Coriolis force averaged over the control volume, $\partial p/\partial x_F$ is the pressure gradient in the direction x_F, and the subscript 0 refers to values without the turbines present. Any imbalance between the momentum supplied to the control volume and total bottom drag (i.e. turbine thrust and surface drag) will accelerate or decelerate the flow, giving the time derivative terms in (2.2) (Nishino & Dunstan 2020). In this study, we ignore the Coriolis terms and time derivative terms (i.e. we assume stationary atmospheric conditions) and

use a fixed definition for the farm-layer height as $H_F = 2.5H_{hub}$, where H_{hub} is the turbine hub height, following Kirby *et al.* (2022).

The theoretical framework that Nishino & Dunstan (2020) used to derive (2.1) is known as the 'two-scale momentum theory'. The left-hand side of (2.1) is expected to depend primarily on turbine-scale or 'internal' conditions. This includes turbine layout and operating conditions, and the hub-height wind speed and direction. The right-hand side of (2.1) is assumed to depend on 'external' farm-scale conditions.

The farm wind-speed reduction factor β can be calculated using (2.1) for a set of C_T^*, γ and M. Using β, the average turbine power coefficients can be calculated using

$$C_p = \beta^3 C_p^*, \tag{2.3}$$

where C_p is the (farm-averaged) turbine power coefficient, defined as $C_p \equiv \sum_{i=1}^{n} P_i / \frac{1}{2}\rho U_{F0}^3 nA$ (with P_i the power of turbine i in the farm), and C_p^* is the (farm-averaged) 'internal' turbine power coefficient, defined as $C_p^* \equiv \sum_{i=1}^{n} P_i / \frac{1}{2}\rho U_F^3 nA$.

3. Momentum availability factor model

The momentum availability factor M describes the increase in momentum supplied to the farm site due to the presence of the turbines. In this study we model this as

$$\begin{aligned} M &= \frac{M_F}{M_{F0}} = 1 + \frac{\Delta M_F}{M_{F0}} \\ &= 1 + \frac{\Delta M_{F,Advection}}{M_{F0}} + \frac{\Delta M_{F,PGF}}{M_{F0}} + \frac{\Delta M_{F,Entrainment}}{M_{F0}}. \end{aligned} \tag{3.1}$$

We introduce new variables M_{F0}, defined as the total net momentum flux into the farm control volume without the turbines present, and M_F, the total net momentum flux with the turbines. Here, ΔM_F is the change in momentum flux due to the presence of the turbines, defined as $\Delta M_F \equiv M_F - M_{F0}$.

This ΔM_F can be decomposed into the contributions from different physical mechanisms. For this study, we will consider only the contributions from net momentum advection, pressure gradient forcing (PGF) and turbulent entrainment as shown in (3.1), which provides a new framework for modelling the impact of farm-scale flows.

In this study, we propose simple analytical models for the components of (3.1). For each component, we consider a control volume of height H_F around the farm. (Note that this control volume can be different from the control volume used to derive (2.1).) The height of the control volume can be chosen arbitrarily, but choosing H_F allows terms to be linked to farm wind-speed reduction factor β. We use a steady quasi-1-D analysis for the advection and PGF terms. The entrainment term is modelled by assuming self-similar vertical shear stress profiles (above the top turbine tip). However, the modelling framework is not specific to the analytical models proposed in the following sections. Equation (3.1) can be a starting point for future studies using more sophisticated approaches for each component.

3.1. *Net momentum advection*

Figure 1 shows a rectangular wind farm control volume, where L is the length of the farm in the hub-height wind direction, and W is the farm width. Using a quasi-1-D approach,

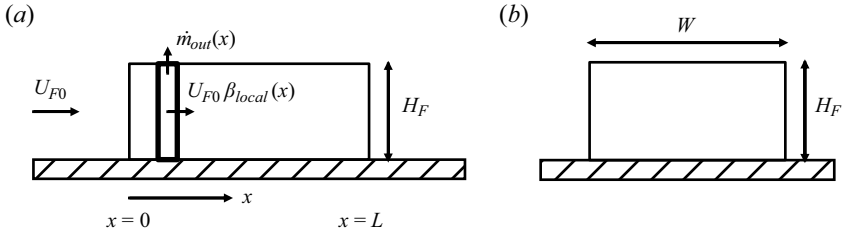

Figure 1. Control volume analysis for net momentum advection calculation: (*a*) side view, and (*b*) front view.

we define the spanwise and vertically averaged wind speed throughout the control volume as $U_{F0}\beta_{local}(x)$. In our notation, $x = 0$ is at the front of the farm, and $x = L$ is at the rear. Note that in figure 1(*a*), $\beta_{local}(0)$ is not exactly equal to 1 since the wind speed decelerates upstream of the farm due to the farm blockage effect. Our proposed model of net momentum advection can therefore capture the impact of farm blockage.

By considering the conservation of mass of an elemental control volume (shown by the bold box in figure 1), the mass flux out of the farm control volume at position x can be expressed as

$$\dot{m}_{out}(x) = -\rho H_F W U_{F0} \frac{\mathrm{d}\beta_{local}(x)}{\mathrm{d}x}. \tag{3.2}$$

Note that this could be mass flux out of the top or sides of the farm control volume, but the flux out of the sides is negligibly small in this quasi-1-D approach (where $W \gg H_F$). The momentum flux into the control volume at the front surface (i.e. $x = 0$) is given by

$$\dot{m}_{in,front}\, U_{in,front} = \rho U_{F0}^2\, \beta_{local}(0)^2\, H_F W, \tag{3.3}$$

noting that a positive value represents a net inflow of momentum. The net momentum flux through the rear surface (i.e. $x = L$) is given by

$$\dot{m}_{in,rear}\, U_{in,rear} = -\rho U_{F0}^2\, \beta_{local}(L)^2\, H_F W. \tag{3.4}$$

The momentum flux through the top surface is the integral of the mass flux and streamwise velocity at each position x, i.e.

$$\dot{m}_{in,top}\, U_{in,top} = -\int_0^L \dot{m}_{out}(x)\, U_{F0}\, \beta_{local}(x)\, \mathrm{d}x. \tag{3.5}$$

We substitute (3.2) into (3.5) and integrate to obtain

$$\dot{m}_{in,top}\, U_{in,top} = \rho U_{F0}^2 H_F W \left[\tfrac{1}{2}\beta_{local}(L)^2 - \tfrac{1}{2}\beta_{local}(0)^2\right]. \tag{3.6}$$

The total net momentum inflow into the control volume is given by the sum of (3.3), (3.4) and (3.6), i.e.

$$\Delta M_{F,Advection} = \tfrac{1}{2}\rho U_{F0}^2 H_F W \left[\beta_{local}(0)^2 - \beta_{local}(L)^2\right]. \tag{3.7}$$

This expression relates the change in momentum advection to the velocity at the front and rear of the farm.

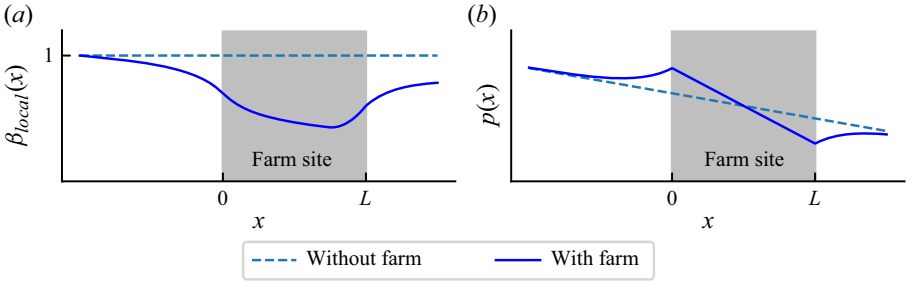

Figure 2. Example variations of (*a*) local farm wind-speed reduction factor $\beta_{local}(x)$, and (*b*) pressure $p(x)$, with streamwise location.

3.2. *Pressure gradient forcing*

The LES results in the literature have shown that large wind farms can induce additional pressure gradients across them (e.g. Allaerts & Meyers 2017; Wu & Porté-Agel 2017; Lanzilao & Meyers 2022). When farms induce additional pressure gradients, commonly a velocity reduction at the front of the farm is observed. This velocity reduction at the front of the farm is known as 'wind farm blockage'. Typically, a velocity increase and pressure reduction at the rear of the farm can also occur. Figure 2 shows example streamwise variations of $\beta_{local}(x)$ and pressure.

In this subsection, we propose a simple model for $\Delta M_{F,PGF}$. We apply Bernoulli's equation as an approximation to link the pressure increase to the velocity reduction at the front of the farm. We neglect changes in gravitational potential energy. It is assumed that changes in pressure are uniform up to the control volume height H_F.

Our aim here is to model an increased pressure difference Δp across the farm. The physical mechanism increasing the pressure difference is not considered directly (e.g. gravity waves) but is included implicitly in Δp, which is composed of a pressure increase Δp_{front} at the front surface of the farm control volume, and pressure decrease Δp_{rear} at the rear surface.

The velocity reduction in front of the farm takes place over a distance $L_{induction}$. Without the farm present, the background pressure force is balanced by the bottom shear stress over this region, i.e.

$$h_0\,\Delta p_0 = \tfrac{1}{2}\rho C_{f0} U_{F0}^2\, L_{induction}, \tag{3.8}$$

where h_0 is the ABL height without the farm present. Therefore, the ratio of friction head loss to dynamic pressure is given by $L_{induction}\,C_{f0}/h_0$. Although $L_{induction}$ can be an order of magnitude larger than h_0, a typical value of C_{f0} for offshore sites is 0.002–0.003. The dynamic pressure is therefore typically one to two orders of magnitude larger than the friction head loss. As such, as a first-order approach, we consider only pressure changes due to changes in dynamic pressure, justifying the use of Bernoulli's equation.

Bernoulli's equation is applied on a streamline from far upstream to the front of the farm. The increase in pressure force on the front surface of the control volume is therefore given by

$$\Delta p_{front}\,H_F W = \tfrac{1}{2}\rho U_{F0}^2 H_F W\left[1-\beta_{local}(0)^2\right]. \tag{3.9}$$

We then assume that $\Delta p_{rear} = \Delta p_{front}$, and therefore $\Delta p = 2\,\Delta p_{front}$. This is a strong assumption, and in reality, this would depend on the atmospheric conditions. The LES results of Wu & Porté-Agel (2017) and Lanzilao & Meyers (2022) show approximately

	$\Gamma = 1$ K km^{-1}		$\Gamma = 5$ K km^{-1}	
	Staggered	Aligned	Staggered	Aligned
$\beta_{local}(0)^2 + \beta_{local}(L)^2$	1.519	1.579	1.361	1.473
$1 + \beta^2$	1.639	1.696	1.548	1.611
Percentage error	7.99 %	7.40 %	13.7 %	9.37 %

Table 1. Percentage errors of approximation $\beta_{local}(0)^2 + \beta_{local}(L)^2 \approx 1 + \beta^2$ using data from Wu & Porté-Agel (2017). Note that Γ refers to the free atmosphere stratification strength.

equal and opposite pressure changes at the front and rear of the farm, suggesting that this approximation is valid. However, the LES of Allaerts & Meyers (2017) and Lanzilao & Meyers (2023) suggest that this assumption is likely to be valid only for certain atmospheric stratifications.

Then $\Delta M_{F,PGF}$ is given by

$$\Delta M_{F,PGF} = \Delta p\, H_F W = \tfrac{1}{2}\rho U_{F0}^2 H_F W \left[2 - 2\beta_{local}(0)^2\right]. \tag{3.10}$$

Combining advection and PGF terms gives

$$\Delta M_{F,Advection} + \Delta M_{F,PGF} = \tfrac{1}{2}\rho U_{F0}^2 H_F W \left[2 - \beta_{local}(0)^2 - \beta_{local}(L)^2\right]. \tag{3.11}$$

Generally, the velocity at the front of the farm is close to the undisturbed value. The velocity at the rear of the farm tends to be close to the farm-averaged value. As a simple first-order approach, we assume that the small velocity reduction at the front of the farm, $1 - \beta_{local}(0)$, is equal to the small increase at the rear (relative to the farm-averaged wind speed), $\beta_{local}(L) - \beta$. As such, we can say that $\beta_{local}(0)^2 + \beta_{local}(L)^2 \approx 1 + \beta^2$. Applying this approximation to (3.11) gives

$$\Delta M_{F,Advection} + \Delta M_{F,PGF} = \tfrac{1}{2}\rho U_{F0}^2 H_F W(1 - \beta^2). \tag{3.12}$$

To check the validity of this approximation, we used data from finite wind farm LES performed by Wu & Porté-Agel (2017). We take the hub-height wind speed normalised by the inflow value as a proxy for $\beta_{local}(x)$. Note that H_F has been defined so that the hub-height wind speed is approximately equal to the farm-layer-averaged speed (Kirby *et al.* 2022). For the four farms simulated by Wu & Porté-Agel (2017), this assumption gives an overestimation of the order of 10 % (see table 1).

Dividing by the initial momentum supply M_{F0} gives

$$\frac{\Delta M_{F,Advection}}{M_{F0}} + \frac{\Delta M_{F,PGF}}{M_{F0}} = \frac{\tfrac{1}{2}\rho U_{F0}^2 H_F W(1 - \beta^2)}{\tau_{w0} LW} = \frac{1}{C_{f0}}\frac{H_F}{L}(1 - \beta^2). \tag{3.13}$$

Although this is an approximation, (3.13) shows that when advection and PGF terms are combined, the dependence on farm inlet and outlet velocities disappears. Interestingly, this suggests that the impact of farm-scale flows may not depend directly on the wind speed at the front of the farm.

3.3. *Turbulent entrainment*

Wind farms increase the turbulent mixing within the ABL. This increases the momentum entrainment into the farm (Stevens & Meneveau 2017). This mechanism supplies

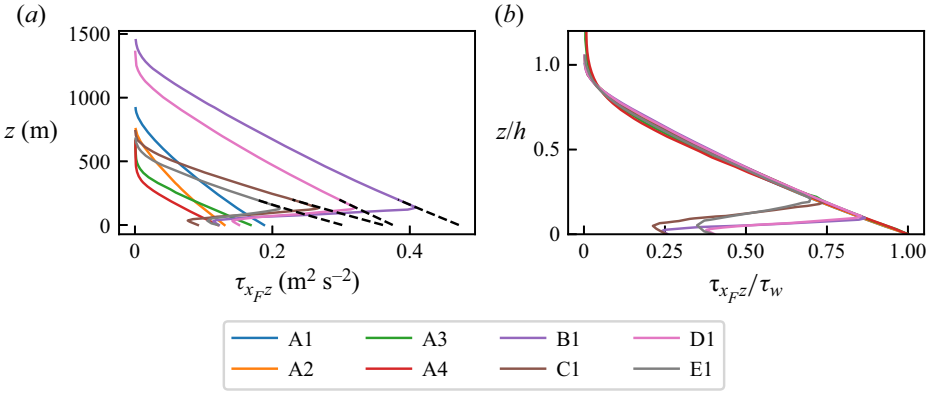

Figure 3. (*a*) Vertical profiles of shear stress from horizontally periodic LES with and without the farm present (Abkar & Porté-Agel 2013). (*b*) Normalised vertical profiles. Note that the legend gives the case names used by Abkar & Porté-Agel (2013).

momentum to the control volume through the shear stress at the top surface. Then $\Delta M_{F,Entrainment}$ can be expressed as

$$\frac{\Delta M_{F,Entrainment}}{M_{F0}} = \frac{\tau_t LW - \tau_{t0} LW}{\tau_{w0} LW} = \frac{\tau_t - \tau_{t0}}{\tau_{w0}}, \tag{3.14}$$

where τ_t is the shear stress at the top of the control volume.

The ABL can be stratified with different profiles of potential temperature, which can change farm performance (Porté-Agel *et al.* 2020). In this study, we consider conventionally neutral boundary layers (CNBLs) because many wind farm LES studies adopted ABLs with these profiles. The CNBLs have self-similar vertical shear stress profiles (Liu, Gadde & Stevens 2021). Therefore, if the surface stress and the boundary layer height are known, then the shear stress at any height can be determined. Note that the height is normalised by $h = h_{0.05}/(1 - 0.05^{2/3})$, where $h_{0.05}$ is the height where the shear stress is 5 % of the surface value.

The self-similarity of shear stress profiles can also be applied to large wind farms. Abkar & Porté-Agel (2013) performed horizontally periodic LES of CNBLs with and without turbines present. Figure 3(*a*) shows the vertical profiles of the shear stress (note that this is the stress in the hub-height wind direction, x_F). Above the turbine top tip (126.5 m in Abkar & Porté-Agel 2013), the vertical profiles have a similar shape. This suggests that the stress profile above the turbines is equivalent to an 'empty' CNBL with a higher surface stress.

The black dashed lines in figure 3(*a*) show the stress profiles above the turbines extrapolated to the surface (using a second-order polynomial regression). This corresponds to the total bottom stress, i.e. surface shear stress and turbine thrust. When the stress profiles of Abkar & Porté-Agel (2013) are normalised by the total bottom stress and new ABL height, they fall onto the same curve (figure 3*b*). This shows that the CNBLs containing wind farms also follow approximately the same self-similar shear stress profile. Figure 3(*b*) shows that wind farms increase the total bottom stress and boundary layer height of CNBLs.

The self-similarity of stress profiles can be used to predict momentum entrainment into large finite-sized wind farms. As a first-order approach, we consider the vertical shear stress profile horizontally averaged across the farm. Figure 4 shows a schematic of the

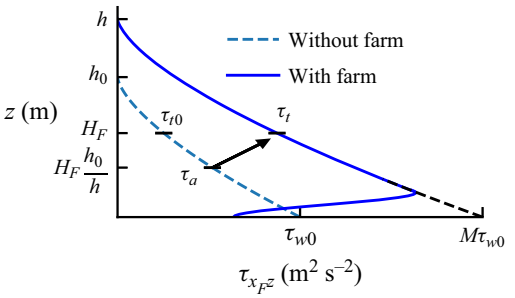

Figure 4. Schematic of vertical shear stress profiles with and without the wind farm.

shear stress profile with and without the farm present. Here, h is the ABL height with the farm present averaged across the farm site. With the farm present, the shear stress is scaled by M and the heights are scaled by h/h_0.

To determine τ_t, we need to calculate the undisturbed shear stress at height $H_F h_0/h$ (denoted as τ_a). This is found by linearly interpolating the stress between the top of the control volume and the surface, i.e.

$$\tau_a = \tau_{w0} - (\tau_{w0} - \tau_{t0})\,\frac{h_0}{h}. \tag{3.15}$$

Whilst the shear stress profile is not strictly linear, it is approximately linear away from the top of the ABL. Then τ_t can be expressed in terms of M and the undisturbed shear stress profile:

$$\tau_t = M\tau_a = M\left(1 - \frac{h_0}{h}\right)\tau_{w0} + M\,\frac{h_0}{h}\,\tau_{t0}. \tag{3.16}$$

Equation (3.16) can be substituted into (3.14) to calculate $\Delta M_{F,Entrainment}$:

$$\frac{\Delta M_{F,Entrainment}}{M_{F0}} = \frac{(\tau_t - \tau_{t0})LW}{\tau_{w0}LW} = M + M\,\frac{h_0}{h}\left(\frac{\tau_{t0}}{\tau_{w0}} - 1\right) - \frac{\tau_{t0}}{\tau_{w0}}. \tag{3.17}$$

The different sources of momentum increase can be summed to calculate M. Substituting (3.13) and (3.17) into (3.1), we obtain

$$M = 1 + \frac{1}{C_{f0}}\,\frac{H_F}{L}\left(1 - \beta^2\right) + M + M\,\frac{h_0}{h}\left(\frac{\tau_{t0}}{\tau_{w0}} - 1\right) - \frac{\tau_{t0}}{\tau_{w0}}, \tag{3.18}$$

which can be rearranged to give

$$M = \frac{1 + \dfrac{1}{C_{f0}}\,\dfrac{H_F}{L}\left(1 - \beta^2\right) - \dfrac{\tau_{t0}}{\tau_{w0}}}{\dfrac{h_0}{h}\left(1 - \dfrac{\tau_{t0}}{\tau_{w0}}\right)}. \tag{3.19}$$

Using (3.1), we can simply sum the different sources of momentum increase. The result is a single equation to model the impact of farm-scale flows on farm performance. Equation (3.19) is an approximate expression for M as a function of β and h/h_0. Different models could be used to predict h/h_0 in this formula for M. In the next subsection, we present a simple first-order model for h/h_0 as a function of β.

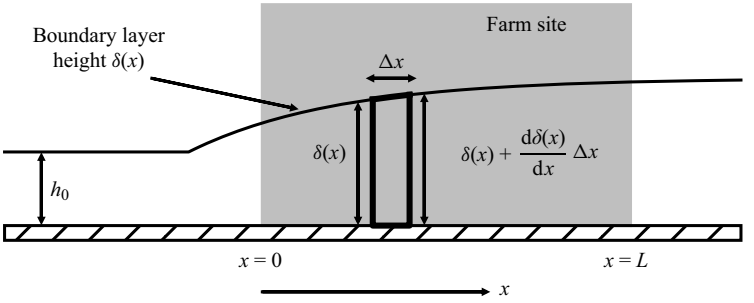

Figure 5. Quasi-1-D control volume analysis for ABL flow over a wind farm.

3.4. *Boundary layer height increase*

In this subsection, we present a simple model for increase in ABL height h/h_0 in response to a wind farm. We use a quasi-1-D analysis of a boundary layer flow over a farm (see figure 5). Here, $\delta(x)$ is the ABL height at streamwise position x. We assume that there is no mass flux between the boundary layer and the free atmosphere above. The quasi-1-D approach neglects the effect of flow bypassing around the sides of the farm.

We consider the conservation of mass across a control volume encompassing a section of the ABL (in bold in figure 5). The velocity averaged over the height of the ABL at position x is denoted $U_A(x)$. We assume that the streamwise variation of $U_A(x)$ is the same as the streamwise variation of $\beta_{local}(x)$. This is strictly not true, but could give a reasonable first-order approximation of $U_A(x)$. Therefore $U_A(x) = U_{A0}\,\beta_{local}(x)$, where U_{A0} is the velocity averaged throughout the undisturbed ABL. The mass flux in through the left-hand side of the control volume is given by

$$\dot{m}_{in} = \rho U_{A0}\,\beta_{local}(x)\,\delta(x)\,W. \tag{3.20}$$

Taking the limit as Δx approaches 0, the mass flux out of the right-hand side is given by

$$\left.\begin{aligned} \dot{m}_{out} &= \rho\left[U_{A0}\,\beta_{local}(x) + U_{A0}\,\frac{\mathrm{d}\beta_{local}(x)}{\mathrm{d}x}\,\mathrm{d}x\right]\left[\delta(x) + \frac{\mathrm{d}\delta(x)}{\mathrm{d}x}\,\mathrm{d}x\right]W, \\ \dot{m}_{out} &= \rho U_{A0}\,\beta_{local}(x)\,\delta(x)\,W + \rho U_{A0}\,\beta_{local}(x)\,\frac{\mathrm{d}\delta(x)}{\mathrm{d}x}\,\mathrm{d}x\,W \\ &\quad + \rho U_{A0}\,\frac{\mathrm{d}\beta_{local}(x)}{\mathrm{d}x}\,\mathrm{d}x\,\delta(x)\,W, \end{aligned}\right\} \tag{3.21}$$

whilst neglecting second-order terms. From the mass conservation, $\dot{m}_{in} = \dot{m}_{out}$, we have

$$\left.\begin{aligned} \rho U_{A0}\,\beta_{local}(x)\,\frac{\mathrm{d}\delta(x)}{\mathrm{d}x}\,W &= -\rho U_{A0}\,\delta(x)\,\frac{\mathrm{d}\beta_{local}(x)}{\mathrm{d}x}\,W, \\ \frac{\mathrm{d}\delta(x)}{\delta(x)} &= -\frac{\mathrm{d}\beta_{local}(x)}{\beta_{local}(x)}. \end{aligned}\right\} \tag{3.22}$$

Both sides of (3.22) can be integrated from far upstream to a given position, resulting in

$$\delta(x) = \frac{h_0}{\beta_{local}(x)}, \tag{3.23}$$

using the condition that far upstream, $\delta(x) = h_0$ and $\beta_{local}(x) = 1$. To find h, $\delta(x)$ is averaged between $x = 0$ and $x = L$ (as h is the ABL height averaged across the wind

	$\Gamma = 1$ K km^{-1}		$\Gamma = 5$ K km^{-1}	
	Staggered	Aligned	Staggered	Aligned
$1/\beta$	1.250	1.200	1.349	1.281
$\frac{1}{L}\int_0^L \frac{\mathrm{d}x}{\beta_{local}(x)}$	1.253	1.202	1.354	1.285
Percentage error	0.244 %	0.160 %	0.414 %	0.248 %

Table 2. Percentage errors of approximation in (3.24) using data from Wu & Porté-Agel (2017).

farm site):

$$\frac{h}{h_0} = \frac{1}{L}\int_0^L \frac{\mathrm{d}x}{\beta_{local}(x)} \approx \frac{1}{\beta}, \tag{3.24}$$

where the relationship between β and $\beta_{local}(x)$ is given by $\beta = \int_0^L \beta_{local}(x)\,\mathrm{d}x$. If $\beta_{local}(x)$ is constant, then the left-hand side of (3.24) is equal to $1/\beta$, which we assume to be true generally. In reality, the more $\beta_{local}(x)$ varies, the less accurate this assumption becomes. If $\beta_{local}(x)$ is close to zero at any point, then the approximation in (3.24) becomes less accurate. To check the validity of this assumption, we again use the LES data from Wu & Porté-Agel (2017). For the four farms simulated by Wu & Porté-Agel (2017), the maximum error of this assumption was approximately 0.4 % (see table 2). Therefore, the approximation is reasonable for realistic profiles of $\beta_{local}(x)$.

The derivation of (3.24) neglects horizontal flow deflections around the farm. This assumption is reasonable so long as the mass flux through the top surface of the farm control volume is much greater than through the sides. The mass flux through the top surface is given by ρwLW (where w is the average vertical velocity through the top surface). The mass flux through the side surfaces is given by $2\rho vLH_F$ (where v is the average lateral velocity at the side surfaces). If we assume that v and w are of similar magnitudes, then neglecting horizontal deflections is reasonable so long as $W \gg H_F$.

Substituting (3.24) into (3.19), we get the following expression for M:

$$M = \frac{1 + \dfrac{1}{C_{f0}}\dfrac{H_F}{L}(1-\beta^2) - \dfrac{\tau_{t0}}{\tau_{w0}}}{\beta\left(1 - \dfrac{\tau_{t0}}{\tau_{w0}}\right)}. \tag{3.25}$$

Equation (3.25) is a single algebraic equation to predict the impact of farm-scale flows on farm performance. It includes the effects of net advection, PGF and turbulent entrainment. The only environmental parameter needed is the undisturbed shear stress profile. Equation (3.25) can be used with the two-scale momentum theory to predict farm power. In § 4, we compare the predictions of farm power output with the results from finite wind farm LES reported in the literature.

4. Comparison with finite wind farm LES

The two-scale momentum theory presented in § 2 can be used to predict wind farm power. For arrays of actuator discs (or aerodynamically ideal turbines operating below the rated wind speed), $C_p^* = \alpha C_T^*$, where $\alpha \equiv U_T/U_F$ (with U_T the streamwise velocity averaged

over the rotor swept area). We can estimate α using the expression $\alpha = \sqrt{C_T^*/C_T'}$, where $C_T' \equiv T_i/\frac{1}{2}\rho U_{T,i}^2 A$ is a turbine resistance coefficient describing the turbine operating conditions. (Note that this is strictly valid only for infinitely large regular arrays of turbines where the thrust of each individual turbine is identical to farm-averaged turbine thrust.). The C_p of an actuator disc is therefore given by

$$C_p = \beta^3 C_p^* = \beta^3 {C_T^*}^{3/2} {C_T'}^{-1/2}. \tag{4.1}$$

Note that when we are considering an isolated turbine, C_T' is related to the classic turbine thrust coefficient by the relation $C_T' = C_T/(1-a)^2$ (where a is the turbine induction factor). Generally, C_T^* depends on the turbine layout, but its upper limit may be predicted by using an analogy to the classical actuator disc theory (Nishino 2016), as

$$C_T^* = \frac{16 C_T'}{(4 + C_T')^2}. \tag{4.2}$$

Note that (4.2), like the classical actuator disc theory, is valid only for induction factors up to 0.5. Since this model predicts an upper limit of C_T^* for a given C_T', it can be used to predict an upper limit to farm performance (Kirby *et al.* 2022). Using this model with $\beta = 1$, the power coefficient of an isolated turbine $C_{p,Betz}$ can also be retrieved as

$$C_{p,Betz} = \frac{64 C_T'}{(4 + C_T')^3}. \tag{4.3}$$

It is important to note that (4.1) and (4.2) are strictly valid only when $U_{T,i}$ is the same for all turbines. However, in this study, we consider only wind farms in which C_T' is the same for all turbines, and in this case, (4.1) and (4.2) can be applied in an approximate manner even when $U_{T,i}$ varies throughout the farm.

We used the new model of M (3.25) with the two-scale momentum theory (2.1) with $\gamma = 2$ to predict wind farm power, i.e. solving

$$\left(C_T^* \frac{\lambda}{C_{f0}} + 1\right)\beta^2 = \frac{1 + \dfrac{1}{C_{f0}}\dfrac{H_F}{L}(1-\beta^2) - \dfrac{\tau_{t0}}{\tau_{w0}}}{\beta\left(1 - \dfrac{\tau_{t0}}{\tau_{w0}}\right)} \tag{4.4}$$

for β, which is then substituted into (4.1) to calculate C_p. The definitions of C_p, C_T^* and C_T' are summarised in table 3.

We compared the predictions against finite wind farm LES results from Wu & Porté-Agel (2017), Allaerts & Meyers (2017) and Lanzilao & Meyers (2022). We selected these studies because they simulated large wind farms (longer than 15 km in the streamwise direction). They published the undisturbed vertical shear stress profile, which is a required input to the model for M. These studies were also selected because the results are normalised by the power of an isolated turbine rather than the front row turbine power. The three studies performed LES of four farms with staggered turbine layouts, and six farms with aligned layouts.

Kirby *et al.* (2022) reported that C_T^* varied with turbine layout due to turbine–wake interactions. The upper limit of C_T^* was predicted well by (4.2). Staggered layouts will tend to have C_T^* values close to this upper limit; hence (4.2) and (4.4) can be used to predict

Symbol	Name	Formula	Note
C_p	Average turbine power coefficient	$\frac{\sum_{i=1}^{n} P_i}{\frac{1}{2}\rho U_{F0}^3 nA}$	U_{F0} is the undisturbed farm-layer-averaged wind speed.
C_p^*	Average 'internal' turbine power coefficient	$\frac{\sum_{i=1}^{n} P_i}{\frac{1}{2}\rho U_F^3 nA}$	U_F is the farm-layer-averaged wind speed with the turbines present.
C_T'	Turbine resistance coefficient	$\frac{T_i}{\frac{1}{2}\rho U_{T,i}^2 A}$	U_T is the wind speed averaged over the rotor swept area.
C_T^*	Average 'internal' turbine thrust coefficient	$\frac{\sum_{i=1}^{n} T_i}{\frac{1}{2}\rho U_F^2 nA}$	Determined by turbine operating conditions and layout.

Table 3. Summary of turbine power and thrust coefficients.

their C_p and give a direct comparison with staggered wind farm LES. Kirby *et al.* (2022) also showed that turbine–wake interactions could reduce C_T^* by up to approximately 20 %, depending on turbine spacings and wind direction. However, the effect of turbine spacing on C_T^* was not studied explicitly for any specific wind direction; therefore, we cannot make a direct comparison with LES of aligned layouts. Nonetheless, we used a 20 % reduced C_T^* value to predict a lower limit for C_p (with the largest turbine-scale loss expected for aligned layouts with a small turbine spacing). This allows a qualitative comparison with LES of aligned wind farms, showing whether our model can capture correctly the observed trends of farm performance under different ABL conditions.

We used the analytical model to predict the farm-averaged power normalised by the isolated turbine power, i.e. $C_p/C_{p,Betz}$. Allaerts & Meyers (2017) and Lanzilao & Meyers (2022) used an actuator disc no-rotation model for the turbines, with $C_T' = 1.33$. For these studies, we used C_T^* from the actuator disc theory (4.2) as an upper limit for C_T^* in (4.4), and then used the expression $C_p/C_{p,Betz} = \beta^3$. For this C_T' value, the actuator disc theory gives $C_T^* = 0.75$. Wu & Porté-Agel (2017) used an actuator disc with rotation implementation for the turbines. As the value of C_T' was unknown, we used the published thrust coefficient curves (Wu & Porté-Agel 2015) to find an upper limit for C_T^*. For the lower limit, we used a 20 % reduced C_T^* value in (4.4) and then the expression $C_p/C_{p,Betz} = \beta^3 0.8^{1.5}$ (assuming that C_T' is unaffected by the turbine layout). Note that this expression comes from (4.1) using a C_T^* value that is 80 % of the upper limit.

Lanzilao & Meyers (2022) normalised the turbine power by the power of an imaginary turbine row 10 km upstream of the farm. However, small reductions in wind speed were observed 10 km upstream for the stratified boundary layer. We instead normalised farm powers from this study by the imaginary upstream power for the neutrally stratified case. This is because the neutrally stratified case had a much smaller reduction in wind speed upstream of the farm. The imaginary upstream turbine power of the staggered and aligned farms in the stratified boundary layer were 6.24 MW and 6.17 MW, respectively (L. Lanzilao, personal communication 2023). For the staggered farm in the neutrally stratified case, it was 6.61 MW (L. Lanzilao, personal communication 2023).

A summary of comparisons between the model predictions and LES is shown in figure 6. Generally, the staggered LES results are close to the upper limits predicted by the two-scale model. The aligned layouts are close to the lower limit of the predictions,

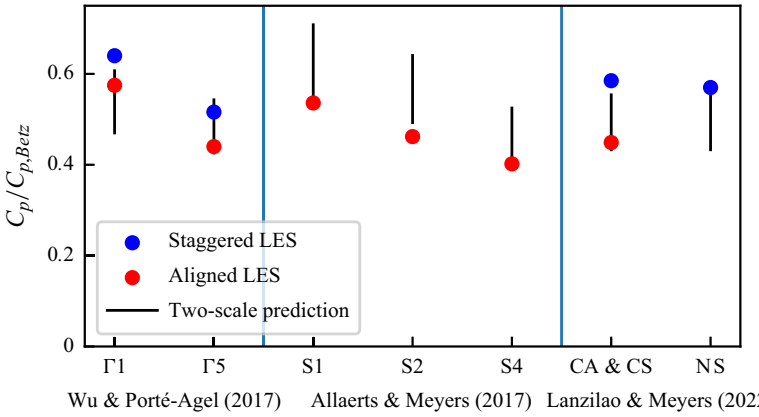

Figure 6. Comparison of farm-average performance predicted by the two-scale model and results from LES. The upper end of each black line corresponds to the upper limit of farm performance predicted by the two-scale model (i.e. without 'turbine-scale loss'), whereas the lower end corresponds to the lower limit predicted assuming that the turbine–wake interaction causes a 20 % reduction of C_T^*.

	Wu & Porté-Agel (2017)		Lanzilao & Meyers (2022)	
	$\Gamma = 1$ K km^{-1}	$\Gamma = 5$ K km^{-1}	CS	NS
λ	0.0160	0.0160	0.0314	0.0314
C_{f0}	0.00557	0.00501	0.00314	0.00314
H_F/L	0.00875	0.00875	0.0188	0.0188
τ_{t0}/τ_{w0}	0.571	0.391	0.475	0.475
β_{model}	0.847	0.816	0.821	0.821
M_{model}	2.41	2.40	5.74	5.74
$C_{p,model}/C_{p,Betz}$	0.607	0.543	0.554	0.554
$C_{p,LES}/C_{p,Betz}$	0.639	0.521	0.585	0.570
$(C_{p,model} - C_{p,LES})/C_{p,LES}$	−5.00 %	4.33 %	−5.39 %	−2.87 %
$(C_{p,model} - C_{p,LES})/C_{p,Betz}$	−3.20 %	2.25 %	−3.15 %	−1.63 %

Table 4. Model parameters and percentage errors in predicting the average power of staggered wind farm LES.

except for the results from Γ1 in Wu & Porté-Agel (2017), where the LES power is higher than the model predictions. The analytical model predicts well the decrease in farm performance with decreasing capping inversion layer height (1000 m, 500 m and 250 m for cases S1, S2 and S4, respectively) observed by Allaerts & Meyers (2017). For the results of Lanzilao & Meyers (2022), the staggered wind farms had very similar performances in the neutral (NS) and conventionally neutral (CS) boundary layers. The two-scale predictions are exactly the same for these two cases because the shear stress profiles were identical.

Note that we made direct comparisons between the two-scale model predictions (without turbine-scale losses) and LES for staggered layouts because these layouts are close to 'optimal' and give a C_T^* value close to the theoretical value given by (4.2) (irrespective of turbine spacing). For the aligned layouts, the exact value of C_T^* depends on turbine spacing, therefore a direct comparison is not currently possible. Table 4 shows the percentage error in farm power predicted for the four staggered farms. When normalised by the farm power

predicted by LES, the error was typically approximately 5 % or less. Normalising by the isolated turbine power predicted theoretically gave errors of approximately 3 % or less.

5. Discussion

This study proposes a novel framework for modelling farm–atmosphere interactions. Equation (3.1) is a general expression for the farm momentum increase as the sum of contributions from different mechanisms. This allows each mechanism to be modelled separately. In this study, we considered contributions from net momentum advection (including farm blockage), PGF and entrainment. Equation (3.1) could provide a framework for combining different or improved models of each mechanism in the future.

We have proposed simple analytical models for each mechanism increasing farm momentum supply. The models make quasi-1-D and steady flow assumptions. The simple momentum availability factor model can be coupled with the two-scale momentum theory to predict farm power. The predictions for staggered farms had a typical error of approximately 5 % or less. The model predictions are for the average power of a finite-sized farm rather than just the power in the fully developed region, i.e. the model captures the effect of the development region and the farm size.

The only environmental parameter required as an input to the model is the undisturbed vertical shear stress profile of the ABL. The model seems to capture most of the impact of ABL height. The proposed model also considers the effect of farm blockage (or the reduction of wind speed upstream of the farm) as part of the advection modelling. This is a physics-based approach to predicting instantly the power of a finite-sized farm without tuning or empirical coefficients.

Our model derivation suggests that the effects of farm blockage and increased PGF could (at least partly) counteract. Note that this is a direct result of our assumption that the pressure changes at the front and rear of the farm are of equal magnitude. A strong free-atmosphere stratification reduces the wind speed in front of the farm (Wu & Porté-Agel 2017; Lanzilao & Meyers 2022). This reduces the net advection of momentum into the farm. When this occurs, an additional pressure gradient tends to be induced across the farm, which increases the momentum supply to the farm. This suggests that the negative effect of farm blockage on the farm power could be somewhat counteracted by the increased PGF. The extent to which these effects counteract will likely depend on atmospheric conditions. For cases NS and CS in Lanzilao & Meyers (2022), the atmospheric conditions are kept constant except for the free-atmosphere stratification. The CNBL case (CS) showed a much greater farm blockage, yet both cases had a similar farm-averaged power, supporting the above argument. The very recent LES study of Lanzilao & Meyers (2023) also suggests that farm blockage often occurs with an increased PGF. However, the degree to which these effects counteract remains unclear. Hence the relationship between farm blockage and PGF seems important and requires further investigation in the future.

Our model can provide physical insight into how farm efficiency changes with atmospheric conditions. Figure 7 shows the predicted values of M and β for the LES studies considered. The model predicts an approximately linear relationship between M and β for a given atmospheric condition, as observed previously by Patel *et al.* (2021). The linear relationship is explained further in Appendix A. For the results of Allaerts & Meyers (2017), S1 had the highest initial inversion layer, and S4 the lowest. Figure 7 shows that the momentum increase (or the value of M) is relatively insensitive to the initial inversion layer height. However, to achieve a certain momentum increase, a lower inversion layer

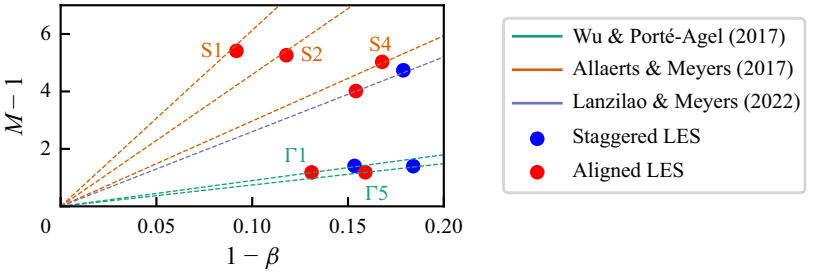

Figure 7. Predicted values of momentum availability factor M and farm wind-speed reduction factor β. Here, β is calculated using (4.4), and M using (3.25), for the flow conditions and farm configuration used in the LES. Note that the lines are calculated using (A5).

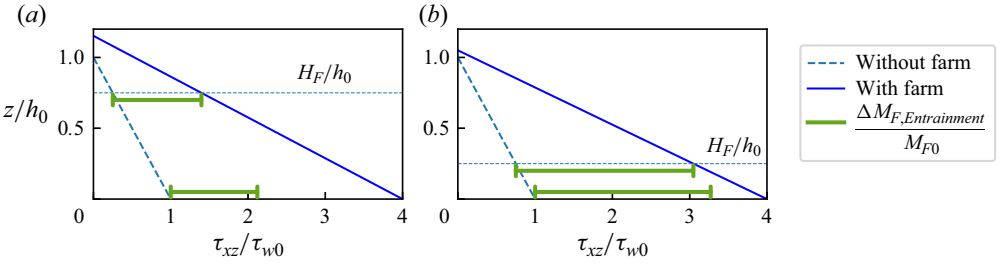

Figure 8. Contribution of entrainment to farm momentum availability factor M for (a) thin initial ABL and (b) thick initial ABL.

has a greater wind-speed reduction (i.e. a larger value of $(1-\beta)$ in figure 7). The lower wind speed results in S4 having a lower farm efficiency than S1 (see figure 6).

A thicker ABL can increase the farm momentum supply with a smaller wind-speed reduction. To illustrate this, we consider the momentum response of two ABLs: a thin ABL (with $H_F/h_0 = 0.75$) and a thick ABL (with $H_F/h_0 = 0.25$). For both ABLs, we use a typical value for large offshore farms of $(1/C_{f0})(H_F/L) = 7.5$, and set $M = 4$ (which means physically that the 'internal' conditions of the farm are adjusted to achieve $M = 4$). The value of β can be calculated using (3.25) for both scenarios. The new and undisturbed shear stress profiles are shown in figure 8. The thin ABL has a smaller entrainment of momentum at the top of the control volume. The top of the control volume is closer to the top of the boundary layer where the velocity shear is lower. Therefore the thin ABL is less efficient at entraining momentum into the farm. With less momentum entrainment, more momentum has to be supplied through advection and PGF in order to achieve the set level of M (see figure 9). These mechanisms increase the momentum supply by reducing the farm-averaged wind speed (3.13). In thicker ABLs, more momentum is supplied to the farm through entrainment, and the advection and PGF supply less momentum. Thicker ABLs can therefore sustain higher wind speeds in the farm and thus have a higher farm efficiency.

This study presents only a preliminary comparison with wind farm LES. To fully validate the proposed model, a comparison with a larger set of LES would be required, which will be the focus of future work. A comparison of model predictions with field observations (such as SCADA data) could also be investigated in future studies. A limitation of the proposed model is that the quasi-1-D analysis captures only the first-order effects. However, the model still gave a close agreement with LES results. More

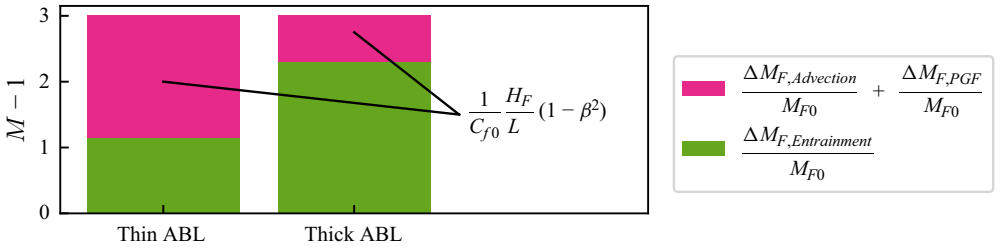

Figure 9. Decomposition of farm momentum availability factor M into entrainment, and advection and PGF terms for (*a*) a thin initial ABL and (*b*) a thick initial ABL. Note that the heights of the green bars in this figure correspond to the widths of the green bars in figure 8.

detailed flow physics was not considered explicitly (e.g. gravity wave excitation) but could be included in future studies. Future work will also aim to predict C_T^* for different turbine layouts and operating conditions. As an example, Legris *et al.* (2023) and Kirby *et al.* (2023) used a wake model to predict C_T^* for different farm designs. Future studies will also focus on the farm–atmosphere interaction under more realistic atmospheric conditions.

It should also be noted that in reality, the assumption of scale separation is not expected to be strictly valid. The entrainment of momentum into the wind farm could depend on the exact turbine layout and not just the farm-average wind-speed reduction. Therefore, to capture higher-order effects, the entrainment component of the model may need some parameters that depend on the internal (turbine-scale) conditions.

6. Conclusions

In this study, we proposed an analytical model of the momentum availability factor for large wind farms. This is a simple model to predict instantly the impact of farm-scale flows on farm performance. This study considered changes in net advection, PGF and turbulent entrainment as the factors contributing to the momentum availability. We derived the model using a steady quasi-1-D control volume analysis and assuming self-similar vertical shear stress profiles. The only environmental parameters required as input to the model are the undisturbed vertical shear stress profiles. We used the new model with the two-scale momentum theory (Nishino & Dunstan 2020) to predict large farm power production. The model compared well with existing LES of finite wind farms in CNBLs. The model captured the impact of ABL height and farm size on farm performance. A direct comparison with LES of staggered farms showed a typical error of 5 % or less.

This study also provides a new framework for modelling farm–atmosphere interactions. The momentum availability factor is expressed as the sum of contributions from different physical mechanisms. As such, the different mechanisms can be modelled separately. We used first-order analytical models for the different components. Despite the simplicity, the model predicts farm power with close agreement to finite wind farm LES. Only one algebraic equation needs to be solved analytically to calculate the farm wind-speed reduction factor β and thus predict farm performance. It also provides a physics-based method to predict farm blockage effects and the impact of ABL height. Future studies could use more advanced models for the different components of the momentum availability factor. This could provide more accurate predictions of wind farm power production.

Acknowledgements. A.K. acknowledges the NERC-Oxford Doctoral Training Partnership in Environmental Research (NE/S007474/1) for funding and training. We also thank Mr L. Lanzilao, Professor J. Meyers and Professor R. Stevens for providing additional data from their studies.

Funding. This work was supported by the Natural Environmental Research Council (NERC) award NE/S007474/1.

Declaration of interests. The authors report no conflict of interest.

Author ORCIDs.
Andrew Kirby https://orcid.org/0000-0001-8389-1619;
Takafumi Nishino https://orcid.org/0000-0001-6306-7702.

Author contributions. A.K. and T.N. derived the analytical model. A.K. made a comparison of the model and existing LES results in the literature, and A.K. wrote the paper with corrections from T.N. and T.D.D.

Appendix A. Approximate expression for wind extractability factor ζ

Patel *et al.* (2021) used twin NWP simulations to calculate M for a realistic wind farm site. They found, for most cases, that M varied almost linearly with the farm induction factor $(1-\beta)$. As such, M can be modelled as

$$M = 1 + \zeta(1-\beta), \tag{A1}$$

where ζ is the 'wind extractability factor' (which is identical to what Nishino & Dunstan (2020) originally proposed as the 'momentum response factor'). Kirby *et al.* (2022) reported that ζ varied with atmospheric conditions and decreased exponentially with wind farm size. The analytical model of M developed in this study can be used to derive an approximate expression for ζ, as (3.25) can be expressed as

$$M = \frac{1}{\beta} + \frac{\dfrac{1}{C_{f0}}\dfrac{H_F}{L}}{1-\dfrac{\tau_{t0}}{\tau_{w0}}}\frac{(1-\beta)(1+\beta)}{\beta}. \tag{A2}$$

This can than be expressed in terms of farm induction factor $(1-\beta)$, e.g.

$$M = \frac{1}{1-(1-\beta)} + \frac{\dfrac{1}{C_{f0}}\dfrac{H_F}{L}}{1-\dfrac{\tau_{t0}}{\tau_{w0}}}\frac{2(1-\beta)-(1-\beta)^2}{1-(1-\beta)}. \tag{A3}$$

The functions of $(1-\beta)$ in (A3) are approximately linear for a realistic range of $(1-\beta)$ (see figure 10). The analytical model of M (3.25) developed in this study therefore predicts the quasi-linear momentum response observed in NWP simulations. We use linear interpolation for $(1-\beta)$ between 0 and 0.2 (a realistic range) to find linear approximations to the functions of $(1-\beta)$. As such, M can be approximated by

$$M_{approx} = 1 + 1.18(1-\beta) + \frac{\dfrac{2.18}{C_{f0}}\dfrac{H_F}{L}}{1-\dfrac{\tau_{t0}}{\tau_{w0}}}(1-\beta). \tag{A4}$$

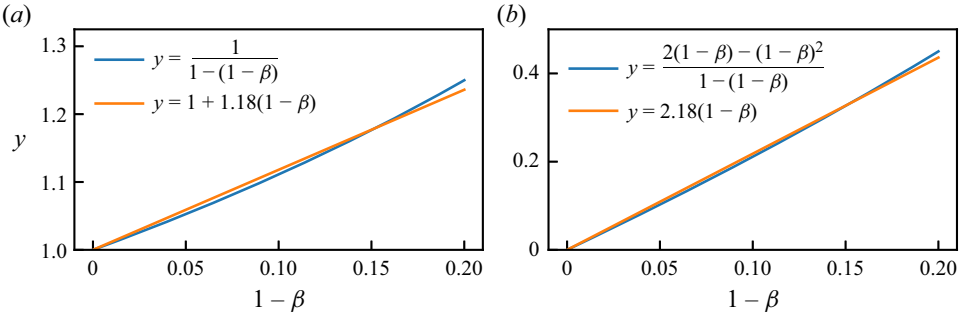

Figure 10. Linear approximations for terms (*a*) $1/(1-(1-\beta))$ and (*b*) $(2(1-\beta)-(1-\beta)^2)/(1-(1-\beta))$ in M expression (A3).

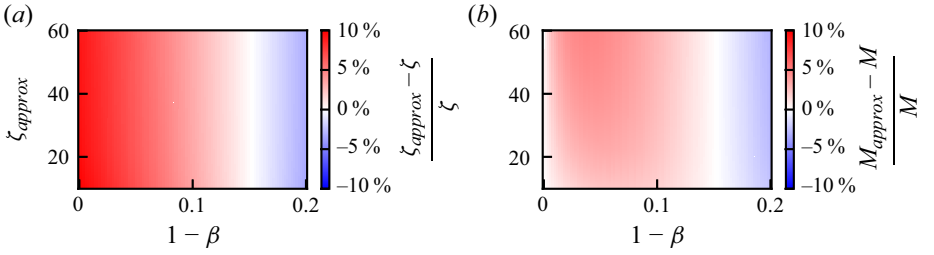

Figure 11. Percentage error of (*a*) ζ_{approx} and (*b*) M_{approx}.

Equation (A4) can be used to derive an approximate expression for ζ, i.e.

$$\zeta_{approx} = 1.18 + \frac{\dfrac{2.18}{C_{f0}}\dfrac{H_F}{L}}{1-\dfrac{\tau_{t0}}{\tau_{w0}}}, \tag{A5}$$

using the expression $\zeta = (M-1)/(1-\beta)$. Equation (A5) predicts the inverse relationship of ζ with farm size reported by Kirby *et al.* (2022). This expression can be simplified further by assuming that the vertical shear stress profile is linear up to the boundary layer height (as assumed in the discussion of figure 8 earlier). The expression for ζ_{approx} then becomes

$$\zeta_{approx} = 1.18 + \frac{2.18 h_0}{C_{f0} L}, \tag{A6}$$

where we refer to L/h_0 as the farm size ratio.

The minimum value of ζ depends on the response of the ABL. If the ABL height is constant (i.e. with a rigid lid), then ζ tends to zero for an infinitely large farm. The minimum value of ζ is non-zero even for an infinitely large farm if the ABL height increases in response to the farm. Differentiating (3.25) (with $L = \infty$) gives

$$\zeta = \frac{\mathrm{d}(M-1)}{\mathrm{d}(1-\beta)} = \frac{1}{\beta^2}, \tag{A7}$$

which gives $\zeta = 1$ for $(1-\beta) = 0$, and $\zeta = 1.56$ for $(1-\beta) = 0.2$. Note that to derive (A6), we performed a linear regression for $0 < (1-\beta) < 0.2$, giving a minimum value of ζ_{approx} of 1.18. Therefore, the minimum value of ζ for realistic ABLs is expected to be 1.

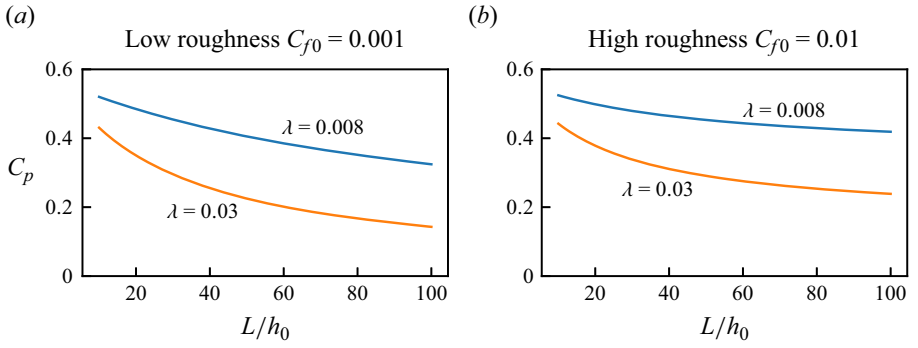

Figure 12. Sensitivity of farm-averaged power coefficient C_p to farm size ratio L/h_0 for low ($\lambda = 0.008$) and high ($\lambda = 0.03$) array densities, for (a) low and (b) high surface roughness values, for a fixed turbine resistance coefficient $C_T' = 1.33$.

The discrepancy between ζ_{approx} and the 'true' ζ (obtained without the linear approximations) is a function of only ζ_{approx} and $(1-\beta)$. Figure 11(a) shows the percentage error of ζ_{approx} for a realistic range of ζ_{approx} and $(1-\beta)$. The maximum error is approximately 10 %, and this occurs for low values of $(1-\beta)$. However, for low values of $(1-\beta)$, the value of M_{approx} is relatively insensitive to the value of ζ_{approx}. Figure 11(b) shows the percentage error of M_{approx}, which is typically less than 5 % for realistic farms.

Appendix B. Sensitivity of farm performance to farm length L

Depending on the farm layout, the streamwise farm length L could vary with wind direction. Hence it is useful to know how the farm power changes with increasing the farm size ratio L/h_0. Equations (2.1), (A1) and (A6) are solved for β, which is then substituted into (4.1). The results are shown for a low surface roughness in figure 12(a), and for a high roughness in figure 12(b). Note that the results in figure 12 are for a C_T' value 1.33 and C_T^* calculated using (4.2). Here, L/h_0 varies from 10 to 100, corresponding to a 10 km long farm in a 1 km ABL height, up to a 30 km long farm in a 300 m ABL height, for example. Figure 12 shows results for farms with both a high array density ($\lambda = 0.03$) and a low density ($\lambda = 0.008$). This corresponds to farms with average turbine spacings $5D$ and $10D$, respectively.

Figure 12 shows that for all scenarios, the farm power decreases with increasing the farm length. The farm power is most sensitive to the farm length for small farm size ratios (i.e. shorter wind farms or thicker ABLs). This suggests that as wind farms become larger, the performance could become less sensitive to wind direction. It should also be noted that the farm power is generally higher when the surface roughness is higher, even though the wind extractability factor decreases as the surface roughness increases (see (A6)). This is because the effective array density λ/C_{f0} decreases as the surface roughness increases (Nishino & Dunstan 2020).

References

Abkar, M. & Porté-Agel, F. 2013 The effect of free-atmosphere stratification on boundary-layer flow and power output from very large wind farms. *Energies* **6**, 2338–2361.

Allaerts, D. & Meyers, J. 2017 Boundary-layer development and gravity waves in conventionally neutral wind farms. *J. Fluid Mech.* **814**, 95–130.

ALLAERTS, D. & MEYERS, J. 2018 Gravity waves and wind-farm efficiency in neutral and stable conditions. *Boundary-Layer Meteorol.* **166**, 269–299.

ALLAERTS, D. & MEYERS, J. 2019 Sensitivity and feedback of wind-farm-induced gravity waves. *J. Fluid Mech.* **862**, 990–1028.

BASTANKHAH, M. & PORTÉ-AGEL, F. 2014 A new analytical model for wind-turbine wakes. *Renew. Energy* **70**, 116–123.

BEMPEDELIS, N., LAIZET, S. & DESKOS, G. 2023 Turbulent entrainment in finite-length wind farms. *J. Fluid Mech.* **955**, A12.

CALAF, M., MENEVEAU, C. & MEYERS, J. 2010 Large eddy simulation study of fully developed wind-turbine array boundary layers. *Phys. Fluids* **22**, 1–16.

DEVESSE, K., LANZILAO, L., JAMAER, S., VAN LIPZIG, N. & MEYERS, J. 2022 Including realistic upper atmospheres in a wind-farm gravity-wave model. *Wind Energy Sci.* **7**, 1367–1382.

FRANDSEN, S. 1992 On the wind speed reduction in the center of large clusters of wind turbines. *J. Wind Engng Ind. Aerodyn.* **39**, 251–265.

FRANDSEN, S., BARTHELMIE, R., PRYOR, S., RATHMANN, O., LARSEN, S., HØJSTRUP, J. & THØGERSEN, M. 2006 Analytical modelling of wind speed deficit in large offshore wind farms. *Wind Energy* **9**, 39–53.

JENSEN, N.O. 1983 A note on wind generator interaction. *Tech. Rep*. Risø-M-2411. Risø National Laboratory.

KATIC, I., HOJSTRUP, J. & JENSEN, N.O. 1986 A simple model for cluster efficiency. In *Proceedings of the European Wind Energy Association Conference and Exhibition, Rome, Italy*, pp. 407–409. Avanti Raguzzi.

KIRBY, A., BRIOL, F.-X., DUNSTAN, T.D. & NISHINO, T. 2023 Data-driven modelling of turbine wake interactions and flow resistance in large wind farms. *Wind Energy* **26**, 968–984.

KIRBY, A., NISHINO, T. & DUNSTAN, T.D. 2022 Two-scale interaction of wake and blockage effects in large wind farms. *J. Fluid Mech.* **953**, A39.

LANZILAO, L. & MEYERS, J. 2022 Effects of self-induced gravity waves on finite wind-farm operations using a large-eddy simulation framework. *J. Phys.: Conf. Ser.* **2265**, 22043.

LANZILAO, L. & MEYERS, J. 2023 A parametric large-eddy simulation study of wind-farm blockage and gravity waves in conventionally neutral boundary layers. *J. Fluid Mech.* (submitted).

LEGRIS, L., PAHUS, M.L., NISHINO, T. & PEREZ-CAMPOS, E. 2023 Prediction and mitigation of wind farm blockage losses considering mesoscale atmospheric response. *Energies* **16**, 386.

LIU, L., GADDE, S.N. & STEVENS, R.J.A.M. 2021 Universal wind profile for conventionally neutral atmospheric boundary layers. *Phys. Rev. Lett.* **126**, 104502.

LUZZATTO-FEGIZ, P. & CAULFIELD, C.P. 2018 Entrainment model for fully-developed wind farms: effects of atmospheric stability and an ideal limit for wind farm performance. *Phys. Rev. Fluids* **3**, 93802.

MENEVEAU, C. 2012 The top-down model of wind farm boundary layers and its applications. *J. Turbul.* **13**, N7.

NISHINO, T. 2016 Two-scale momentum theory for very large wind farms. *J. Phys.: Conf. Ser.* **753**, 032054.

NISHINO, T. & DUNSTAN, T.D. 2020 Two-scale momentum theory for time-dependent modelling of large wind farms. *J. Fluid Mech.* **894**, A2.

PATEL, K., DUNSTAN, T.D. & NISHINO, T. 2021 Time-dependent upper limits to the performance of large wind farms due to mesoscale atmospheric response. *Energies* **14**, 6437.

PORTÉ-AGEL, F., BASTANKHAH, M. & SHAMSODDIN, S. 2020 Wind-turbine and wind-farm flows: a review. *Boundary-Layer Meteorol.* **174**, 1–59.

SMITH, R.B. 2010 Gravity wave effects on wind farm efficiency. *Wind Energy* **13**, 449–458.

STARKE, G.M., MENEVEAU, C., KING, J.R. & GAYME, D.F. 2021 The area localized coupled model for analytical mean flow prediction in arbitrary wind farm geometries. *J. Renew. Sustain. Ener.* **13**, 033305.

STEVENS, R.J.A.M., GAYME, D.F. & MENEVEAU, C. 2016 Generalized coupled wake boundary layer model: applications and comparisons with field and LES data for two wind farms. *Wind Energy* **19**, 2023–2040.

STEVENS, R.J.A.M. & MENEVEAU, C. 2017 Flow structure and turbulence in wind farms. *Annu. Rev. Fluid Mech.* **49**, 311–339.

VAN STRATUM, B., THEEUWES, N., BARKMEIJER, J., VAN ULFT, B. & WIJNANT, I. 2022 A one-year-long evaluation of a wind-farm parameterization in HARMONIE-AROME. *J. Adv. Model. Earth Sy.* **14**, e2021MS002947.

VEERS, P., *et al.* 2019 Grand challenges in the science of wind energy. *Science* **366**, eaau2027.

VEERS, P., *et al.* 2022 Grand challenges: wind energy research needs for a global energy transition. *Wind Energy Sci.* **7**, 2491–2496.

WU, K.L. & PORTÉ-AGEL, F. 2017 Flow adjustment inside and around large finite-size wind farms. *Energies* **10**, 2164.

WU, Y.T. & PORTÉ-AGEL, F. 2015 Modeling turbine wakes and power losses within a wind farm using LES: an application to the Horns Rev offshore wind farm. *Renew. Energy* **75**, 945–955.

ZONG, H. & PORTÉ-AGEL, F. 2020 A momentum-conserving wake superposition method for wind farm power prediction. *J. Fluid Mech.* **889**, A8.